An analysis of ground-based polarimetric sky radiance measurements

Brian Cairns[a], Barbara E. Carlson[a], Andrew A. Lacis[a] and Edgar E. Russell[b]

[a] Goddard Institute for Space Studies, 2880 Broadway, New York, NY 10025
[b] SpecTIR Corporation, Goleta, CA

ABSTRACT

A parametric analysis of sky radiance and polarization measurements based on a database of calculations indicated that there was information contained in the measurements that was not captured by the database. We therefore developed an iterative algorithm for retrieving a size distribution and size resolved refractive indices of aerosols from cloud free measurements of polarized sky radiances. Preliminary results indicate that it is possible to retrieve a size resolved refractive index for a wide range of aerosol sizes, aswell as an aerosol size distribution.

Keywords: Inverse problems, polarization, aerosols

1. INTRODUCTION

Evidence that tropospheric aerosols can cause a direct radiative forcing comparable in magnitude, though opposite in sign, to the expected climate forcing by greenhouse gases[1,2] makes a compelling case for improved efforts to obtain accurate information about the distribution of tropospheric aerosols and their radiative impact[3]. The only method by which we would expect to obtain a global picture of the magnitude and variability of aerosol properties is from satellite measurements. As discussed by Wang and Gordon[4], the retrieval of aerosol optical thickness using satellite reflectance measurements requires an aerosol model, namely the specification of the aerosol scattering phase function and single-scattering albedo. Most often the scattering properties are modeled using Mie theory, which is valid only for spherical particle shape, because shape information is unavailable. However, as shown by Mishchenko *et al.*[5] even moderate nonsphericity results in substantial errors in the retrieved aerosol optical thickness if the data are analyzed using Mie theory. Further, even for spherical particles, it is essential to determine whether the aerosols are absorbing (e.g., biomass burning) or not (e.g., sulfate) to correctly determine the aerosol forcing. Moreover, as we discuss below erroneous assumptions about shape can lead to significant errors in the inference of absorption. It is therefore important for the effective use of satellite reflectance measurements to have a reliable global climatology of aerosol single scatter properties and the ability to cross check satellite retrievals of aerosol properties against other, more accurate measurements.

The only current remote sensing method that can retrieve both a plausible particle size distribution, surface albedo and an average complex refractive index is the combined measurement of the solar direct beam and the diffuse sky radiance[4,6,7]. This type of measurement is made on a routine basis by a worldwide network (AERONET) of instruments[8]. There are however problems with these retrievals in that uncertainty in the calibration of the sky radiometer used for these measurements can cause serious biases. By contrast polarization is a relative measurement and so the accuracy with which it can be measured is limited only by the care with which the instrument used in its measurement is designed and characterized. Indeed there are a significant number of instruments in the AERONET network that measure polarized sky radiances, though there has thus far been little attempt at analysis of these measurements[9].

The difference in the quality of information available from intensity and polarization measurements is illustrated in a simple way in Figure 1. To construct this figure we calculated the distribution of intensity and polarization for an almucantar scan with a solar elevation of 30° and measurements made every 5° in azimuth, for a series of models. The calculations are made for a wavelength of 870 nm with the appropriate Rayleigh optical depth of 0.015 above the aerosol layer and a Lambertian surface below it. We assumed an aerosol size distribution given by the gamma distribution[10] with an effective variance of 0.1. The base conditions for the aerosol layer are an optical depth of 0.1, an effective radius of 0.45 μm, a refractive index of $1.45+0.0i$ and a surface albedo of 0.1. We then allowed different pairs of parameters to vary simultaneously. The vertical and horizontal lines show the location of a "true" model which we are trying to retrieve. The contours around the intersection of these dashed lines show the domains for which the "true" model is indistinguishable from other models and therefore

represents the uncertainty in the retrieval. Two contours are shown on each figure. The solid line contour is drawn assuming that the expected RMS deviation of the measured polarization from the actual polarization is 0.2%. The dashed line contour is drawn assuming that the expected RMS deviation of measured intensity from actual intensity is 5.0%. It is apparent that a reasonable retrieval of size and optical depth is obtained from intensity only measurements, provided the complex refractive index and surface albedo are well constrained *a priori*. This is in agreement with the results of Nakajima *et al.*[7] who found that the inference of optical depth from sky radiance measurements was less susceptible to calibration errors than the inference of optical depth from direct beam measurements. When we examine the simultaneous retrieval of real and imaginary parts of the refractive index and the surface albedo from a full almucantar scan we see that large errors in the inference can be made if only intensity measurements are used. These parameters can, however, be retrieved if accurate polarization measurements are made. Our choice of contour levels is based on the expected uncertainty in a single polarization measurement ~0.2% and the expected uncertainty in the calibration of radiometric measurements ~5%[8].

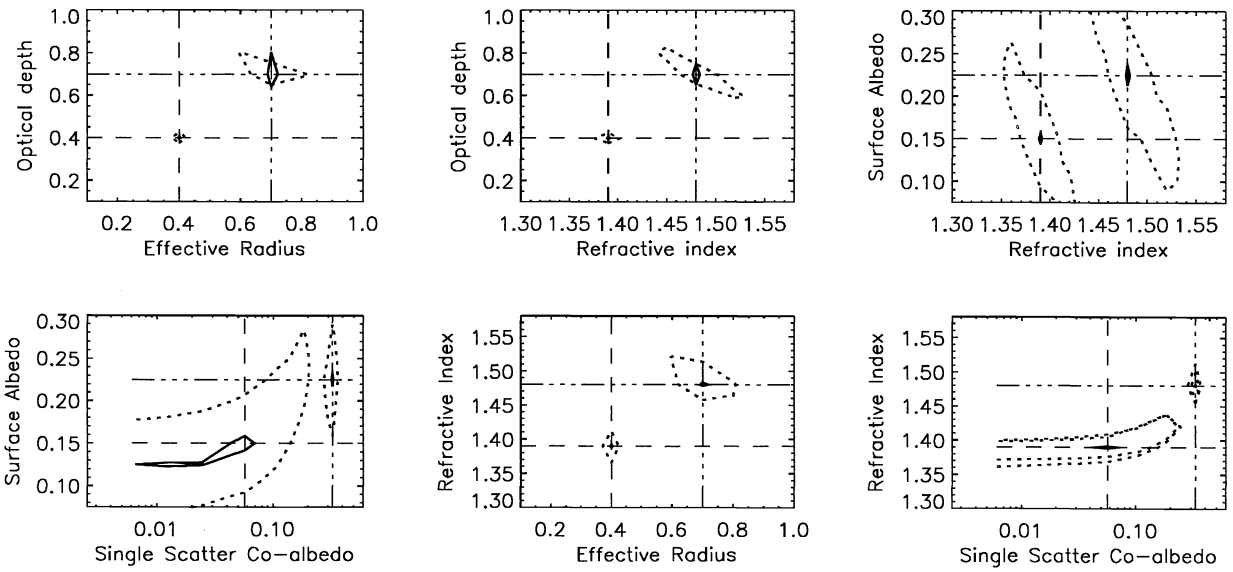

Figure 1. Showing the domains of plausible retrievals using intensity with a calibration uncertainty of 5% (dashed lines) and polarization with an uncertainty of 0.2% (solid lines), for a range of different aerosol microphysical properties.

In order to effectively deal with atmospheric aerosols it is also necessary to be able to recognize the presence of nonspherical particles. This is because the phase function of a non-spherical particle can be mimicked by increasing the real and imaginary parts of the refractive index of a spherical particle of the same surface equivalent size[11]. Figure 2 shows three elements of the phase matrix for a shape mixture of nonspherical particles[12] (solid line) and a polydispersion of spheres (dashed line) with the same size distribution and refractive index of 1.53+0.0055*i* at a wavelength of 550nm. The phase function behavior of the nonspherical particles is well approximated by a polydispersion of spheres (asymmetry parameters of 0.73 and 0.74 respectively) with the same size distribution as the nonspherical particles and a refractive index of 1.95+0.02*i* (dot-dashed line). However the polarization properties (-F12/F11) are not well modelled by spheres with a spuriously large refractive index and the single-scatter coalbedo is overestimated by 300%. The inability to simultaneously match intensity and polarization measurements of non-spherical particles with surface equivalent spheres suggests that it should be possible to differentiate between non-spherical and absorbing particles, using polarimetric measurements.

Although it has long been appreciated that both the surface albedo and aerosol microphysical properties and loading have a significant effect on polarization[13,14], ground based polarimetric sky radiance measurements have provided few quantitative results, notable exceptions being surface albedo retrievals[15] and vertical profiles of stratospheric aerosols[16]. The principal application of polarimetric information in earth based measurements thus far has been for in-situ measurements, where the modelling of the polarization only requires single-scattering calculations[17,18,19]. Indeed some of the refractive index information

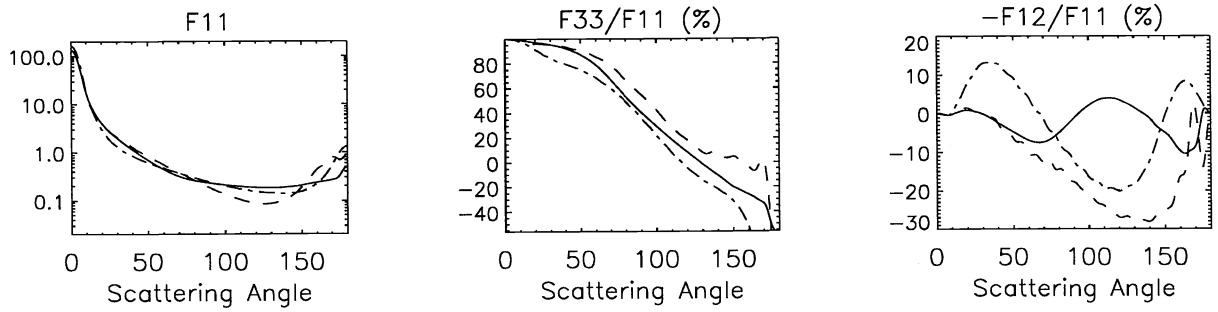

Figure 2. Phase matrix elements for a shape and size mixture of nonspherical particles with a refractive index of 1.53+0.0055*i* (solid line), for a surface equivalent size distribution of spheres with the same refractive index (dashed line) and for a surface equivalent size distribution of spheres with a refractive index of 1.95+0.02*i* (dot-dashed line).

that will be used in proposed aerosol retrieval algorithms[20] and is used in aerosol climatologies[21] was derived from polar nephelometer measurements[17,18,22]. Factors which may have been responsible for the limited interest in polarimetry as a remote sensing tool in the past are the relative complexity and computational intensity of the analysis models. However, effective methods for handling single and multiple scattering of polarized light in the atmosphere have been developed[10,23,24] which, combined with the rapid increase in computer speed and memory of typical workstations, have brought detailed polarization analysis well within the reach of relatively modest computational resources. It should be noted that since polarization is an intrinsic property of light, unless it is included in the analysis of intensity measurements, unexpected errors may occur[25,26]

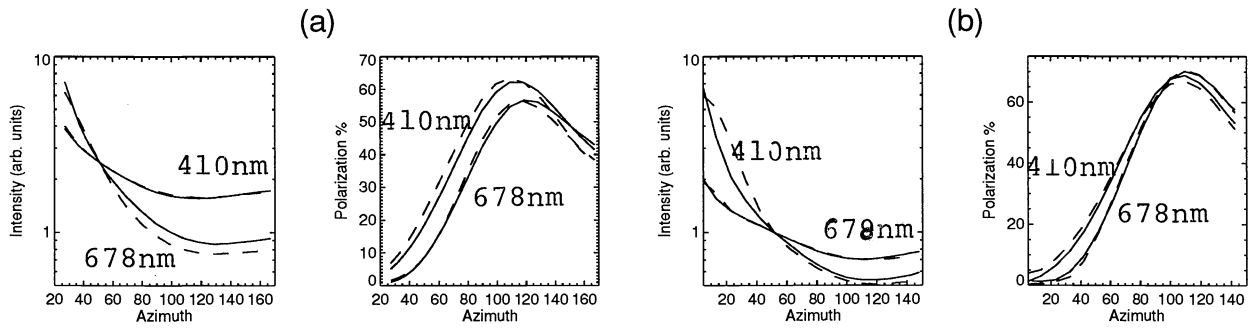

Figure 3. Intensity and polarization of downwelling skylight at 410nm and 678nm (solid line) and theoretical fit based on a table look up of aerosol models (dashed line).

In order to examine whether a parametric estimation of aerosol properties similar to that presented in Figure 1 would be adequate for the purposes of analyzing polarized sky radiance measurements we modified the Galileo PhotoPolarimeter Radiometer (PPR) engineering spare to make it suitable for the acquisition of sky radiance and polarization data. An example of the type of almucantar measurements that we made is shown in Figure 3. The data were acquired in Goleta CA. The figures show the data (solid lines) and the model fit (dashed lines) at 410nm and 678nm. The assumed aerosol size distribution used is a single mode gamma distribution[10] with an effective variance of 0.1 and the single scatter albedo was assumed to be unity. A database of 625 multiple scattering calculations was then generated as a function of real refractive index, effective radius, surface albedo and optical depth at both wavelengths and an overall best fit for both intensity and polarization at 410nm and 678nm was found. The data in Fig. 3a was obtained on 4th April 1996 and has a best fit for an effective radius of 0.3μm, a refractive index of 1.5 an optical depth (@550nm) of 0.06 and a surface albedo of 0.1. The data in Fig. 3b was obtained on 21st October 1996 and has a best fit for an effective radius of 0.5μm, a refractive index of 1.4

an optical depth (@550nm) of 0.02 and a surface albedo of 0.15. The only correlative information available to check the results found in this analysis of polarization were surface albedo estimates made from AVHRR channels 1 and 2, which were in agreement with the inferred surface albedo. It is however apparent from Figure 3 that the residual differences between the best fit from our database and the data are sufficiently large that more information about the aerosol microphysical properties is present in the data than is represented in our database.

In this paper we describe an iterative method that allows us to retrieve this information, viz., the aerosol size distribution and a size resolved refractive index, from measurements of the sky radiance and polarization. The method is similar to those presented by Wang and Gordon[4] and by Nakajima *et al.*[7], but casts the iterative method in a more general framework and also makes use of the polarization of skylight so that it is possible to retrieve a size resolved estimate of refractive index. In the second section of this paper we describe the vector radiative transfer code that is used in the multiple scattering calculations, since it is only if this code is sufficiently fast that an iterative inversion method is possible. We then briefly note the available methods for retrieving a size distribution and a size resolved refractive index from an inversion of measurements of the phase matrix[17,18,19]. The combination of these two aspects of the iterative method, the multiple scattering calculation and the inversion of the phase matrix, into a technique for inverting measurements of the intensity and polarization of downwelling radiation to obtain aerosol microphysical properties is then outlined. In section 3 simulated retrievals of aerosol properties for a range of aerosol size distributions and refractive indices are presented. Our conclusions on the effectiveness of the method are given in section 4.

2. RETRIEVAL METHOD

2.1 VECTOR DOUBLING/ADDING CODE

The modified vector doubling/adding code[10] that we have developed is sufficiently fast (~10 sec. for a two layer atmosphere) that it can be used in an iterative scheme. The algorithm used is essentially the same as that presented by Hansen and Travis[10] and the modifications, which improve speed and accuracy are based on the work of de Haan *et al.*[24]. Like most multiple scattering algorithms, a Fourier decomposition in azimuth is used to simplify the calculation since successive Fourier components are independent of one another and the decomposition usually reduces the computational burden and storage requirements[24]. This is principally because angular integrations are one, rather than two, dimensional. One problem with the Fourier decomposition in azimuth of the radiance field is that when large particles are present it may require a large number of Fourier terms to accurately describe the radiation field. This problem is mitigated by the observation that multiple scattering tends to wash out sharp scattering features. Thus we would expect the high frequency, high index, Fourier terms in the expansion of the radiance field to be dominated by low order scattering, ie. first and second order scattering events. The Fourier decomposed single scattering contribution is therefore subtracted out of each Fourier term in the decomposition of the radiance field. It can then be added back in exactly when it is required to calculate the radiance at a particular observation point. The Fourier decomposition can therefore be terminated when the radiance field is well approximated by single scattering at some Fourier index which we will denote M_1. Although for Fourier indices lower than M_1 the radiance is not sufficiently accurately modelled using a single scattering approximation the Fourier terms with index lower than M_1 will be well approximated by a second order scattering approximation down to some Fourier index M_2 at which point a full doubling calculation is required to accurately evaluate the radiance.

Thus the calculation is broken up into three stages. A doubling calculation for Fourier indices from zero to M_2, a second order calculation from M_2 to M_1 and then exact evaluation of the single scatter contribution for actual observation points. The speed of the calculation is determined by M_2 since the slowest part of the calculation is the doubling, while the storage requirements are determined by M_1 since it is at this index that the Fourier decomposition is terminated. Although de Haan *et al.*[24] provide useful analytic estimates for M_2 and M_1 based on a generalized spherical function decomposition of the phase function their estimates are not used here, because the requirement that the radiative transfer code be used in an iterative reduction of observational data means that a phase function tabulated at a sufficient number of scattering angles is the preferred form[10]. Estimates of M_2 and M_1 can however be made as part of the multiple scattering calculation. Since the second order scattering calculation is much faster than a doubling calculation there is a negligible computational burden in evaluating the second order scattering at the end of each doubling calculation. The root mean square (RMS), or absolute difference between the doubling calculation and the second order calculation can then be evaluated. As this difference decreases with Fourier index, once it is less than the required computational accuracy we have reached index M_2 and the

doubling calculation is terminated and only second order scattering calculations are performed for higher Fourier indices. The index M_1 is evaluated in a similar way by evaluating the RMS or absolute difference between the second order scattering calculation and the single scattering calculation for Fourier indices greater than M_2. Once the difference is less than the required computational accuracy we have reached index M_1 and the multiple scattering calculation is finished.

The other parameter which must be selected for the doubling calculations is the initial optical depth at which to start the doubling procedure. We use the observation of de Haan *et al.*[24] that in doubling from an initial optical depth τ_0 to some optical depth τ the absolute error grows approximately linearly with τ as long as $\tau<1$ and then saturates for $\tau>1$. The exception is for conservative scattering for the first term in the Fourier decomposition in which case the error continues to grow linearly with τ for $\tau>1$. We use a very conservative initial starting optical depth for the first Fourier term and then determine the starting optical depths to be used for higher Fourier indices numerically. We initialize the doubling calculation with a second order scattering calculation for τ_0. Since the second order scattering calculation is very fast we can evaluate the absolute difference between the results from each doubling step (n) and a second order calculation for that optical depth ($2^n\tau_0$). We can then estimate the final error that would have been made had we started the doubling calculation at that optical depth ($2^n\tau_0$) by multiplying the absolute error by the expected linear growth τ/τ_0. The optical depth ($2^n\tau_0$) prior to this estimated final error being greater than the required computational accuracy is then the initial optical depth used in subsequent doubling calculations. Once the estimated final error is greater than the required computational accuracy the second order calculation for comparison with each doubling step can be terminated. This procedure could be used for each Fourier term since we expect that the required initial optical depth will increase with increasing Fourier index. However for optical depths typical of aerosols there was no increase in computational speed obtained by using this estimate of starting optical depth beyond that estimated from the first Fourier component, since the computational overhead in determining the next starting optical depth offset the increase in speed obtained by doubling from a larger optical depth.

The model atmosphere that is used in these calculations is a two layer atmosphere with a pure molecular layer above a pure aerosol layer above a Lambertian surface. This atmospheric model has been used by Wang and Gordon[4] and can be regarded as a reasonable model of the vertical distribution of scattering properties for a region with a persistent marine inversion. This model can be easily modified to include different vertical profiles and surface bidirectional reflectances if additional information from aircraft measurements, or lidars is available.

The downwelling radiation at the surface is calculated following de Haan *et al.*[24]. When the aerosol layer is added to the surface the downwelling radiation at the surface, $\mathbf{D}_{AER}$, is automatically evaluated as part of the adding calculation. The molecular layer is then added to the aerosol+surface layer and the downwelling radiation $\mathbf{D}_{MOL}$ between the aerosol and molecular layers is automatically calculated as part of the adding calculation. The downwelling radiation at the surface is then calculated from the expression

$$D=D_{AER}\exp(-\tau_{MOL}/\mu_0)+\exp(-\tau_{AER}/\mu)D_{MOL}+D_{AER}*D_{MOL} \quad (1)$$

where the matrix multiplication and angular integration are implicit in the third term on the right hand side of this equation, μ and μ_0 are the viewing and solar zenith angles respectively and τ_{AER} and τ_{MOL} are the aerosol and molecular scattering optical depths respectively. The extension of this algorithm to calculate downwelling and/or upwelling radiation at the interface of any two layers for any total number of layers is trivial[24].

2.2 INVERSE METHODS FOR LINEAR EQUATIONS

The inversion of spectral extinction[27,28,29,30] and single scattering measurements[17,18,19,31] to retrieve aerosol size distributions and refractive indices has been an area of considerable study and we defer to the excellent monograph on the subject for a review of methods[32]. Here we briefly discuss the methods that we use and the reasons for our choices. The scattered light, or the spectral extinction can be written as

$$g(x)=\int K(x,r)f(r)dr \quad (2)$$

where $\mathbf{g(x)}$ represents the scattered radiation field at a scattering angle θ and/or the optical extinction at a wavelength λ. $\mathbf{K(x,r)}$ is an optical scattering kernel, or optical extinction cross section[33]. We assume that the particles are spherical and that their scattering properties can be modelled by Mie theory. Based on Fig. 2 above we expect that excessive errors in the final

fit for intensity and polarization indicate the presence of nonspherical particles. The function **f(r)** is the particle size distribution function dN/dr or simply the number concentration of particles within a size range r to r+dr taken as a function of r. It is the objective of the inversion algorithm to retrieve the distribution **f(r)** from measurements **g(x)**. The integral equation (2) can be either discretized[30], or parameterized[29] to obtain a matrix equation

$$g_j = K_{ji} f_i + \epsilon_j \tag{3}$$

where summation over repeated indices is implied and the ε_i represent noise, or other uncertainties in the data. As has been discussed at length elsewhere the direct inversion of such equations is generally unstable because of the small singular values of the matrix $\mathbf{K_{ji}}$. This means that any noise in the measurements will be hugely magnified by being divided by the very small singular values. Thus, one must attempt, by some method, to select reasonable solutions. This is done by applying constraints on the solution. The constrained solution is derived as follows: Consider first of all the quadratic form given by

$$Q = f_j H_{ji} f_i \tag{4}$$

The value of **Q** is obviously dependent on the vector **f** and on the elements in the matrix **H**. In eq.(3) it can be assumed that an upper bound **E** can be specified for the norm of the noise vector ie. $\mathbf{E}=\varepsilon.\varepsilon$. We now let the vector **f** vary within the limits defined by the upper bound **E** and consider the minimum attained by the quadratic form in eq.(4). The Lagrange multiplier solution to the problem is

$$f = \frac{K^T g}{K^T K + \gamma H} \tag{5}$$

A matrix **H** can now be selected to constrain the solution **f**, by noting that the solution given by eq.(5) is obtained by minimizing **Q**. Any matrix **H** which gives large values of **Q** for oscillatory solutions will therefore force **f** to be smooth. For example the norm of the second differences, or any other differential form for **H** would tend to enforce a smooth solution. Alternative derivations of this equation can obtained by determining the best linear estimator of **f** from the data **g**, given the noise ε. This leads to a similar form for the retrieved size distribution to eq.(5), but with the constraint term given in terms of the inverse of the covariance matrix of the expected size distribution and the covariance of the noise spectrum. Once a smoothness constraint is chosen the only remaining choice in the application of this method is that of the Lagrange multiplier γ. The selection of this parameter can be made based on the requirement that the solution **f** be positive and an additional χ^2 constraint. King[28] has presented an iterative solution of eq.(5) that uses this approach and provides good results. There has however been much discussion about the selection of the regularizing parameter γ[29,30], suffice to say, those aspects of a solution that are sensitive to which of the many criteria is used are not really retrievable.

The other method for retrieving **f** that is commonly used[7] is a nonlinear method that has been developed by Twomey[32]. Its implementation is very simple and if it is applied to the scattered intensity, for which the scattering kernel $\mathbf{K_{ij}}$ is positive, it will always retrieve a positive function **f** provided the staring point is positive. The estimation of the first guess solution is particularly important for this algorithm since a poor first guess can lead to divergence away from a solution, or a limit cycle[17]. We found that for the analysis of linear polarization for which the kernel $\mathbf{K_{ij}}$ is not positive there were no advantages to the nonlinear algorithm since it will not necessarily retrieve a positive function **f**, can be unstable and the solution is strongly dependent on the chosen starting point. In fact we found that even reducing γ to zero in eq.(5) and imposing positivity constraints on **f**[34] provided better solutions than the nonlinear method.

We have therefore restricted the inversion methods for single scattering data to the solution of eq.(5) using King's method[28] and the inversion of eq.(5) with γ=0, but imposed positivity constrain[34]. Amato *et al.*[29] found that both methods gave similar results for the inversion of spectral extinction data. These methods are applied to the simultaneous retrieval of a parameterized size distribution which consists of nineteen log normal distributions geometrically spaced between 0.07 and 8.8 μm with a log variance of 0.25, for each of the refractive indices 1.35, 1.4, 1.45, 1.5 and 1.55. Since the simulations to which these methods are applied consist of thirty six measurements of intensity and polarization the inverse problem is underconstrained (19x5>2x36). Although there may well be better ways to estimate a size resolved refractive index than this type of brute force approach, the simulations shown later demonstrate that it works adequately and provides some insight into what other approaches may be more efficient and reliable.

2.3 INVERSION OF MULTIPLE SCATTERING DATA

In the inversion of measurements of multiply scattered light we are seeking a solution to the equation

$$d^m(\theta) - D(X;\theta)s = 0 \tag{6}$$

where **X** denotes the vector of single scattering properties of the aerosol: **P**(θ), the phase matrix, ϖ the single scatter albedo and τ the optical depth. $\mathbf{d}^m(\theta)$ is the measured Stokes vector at some set of angles θ, **D** is the downwelling radiation matrix and **s** is the Stokes vector of incident solar radiation. In order to solve this equation we usually start with some initial value of the single scattering properties of the aerosol $\mathbf{X}^0$, which is based on a table look up (eg. Fig. 1), complementary measurements (eg. sunphotometry for estimates of aerosol optical depth), or climatological values. The starting value $\mathbf{X}^0$ does not usually provide a perfect fit the data and so to improve the fit we wish to modify $\mathbf{X}^0$. We can rewrite eq.(7) in the form

$$d^m(\theta) - D(X^0 + (X - X^0);\theta)s = 0 \tag{7}$$

Provided $\mathbf{X}-\mathbf{X}^0$ is sufficiently small, ie. we are at least in the neighbourhood of a true solution, this equation is well approximated by the first order Taylor series expansion

$$d^m(\theta) - D(X^0;\theta)s + \frac{\delta D(X;\theta)s}{\delta X}\Big|_{X=X^0}(X - X^0) = 0 \tag{8}$$

The neglect of terms of higher order than the first in this expansion means that the value for **X** that is obtained from equation (8) will not be the true value. It should however be closer to **X** than $\mathbf{X}^0$. This leads to the iterative equation for determining **X** known as the Newton Raphson method viz.,

$$X^{n+1} = X^n - \left[\frac{\delta D(X;\theta)s}{\delta X}\Big|_{X=X^n}\right]^{-1}(d^m(\theta) - D(X^n;\theta)s) \tag{9}$$

The only remaining difficulty in applying this method is determining the functional derivative in eq.(9), or some approximation to it. For the sake of simplicity we will assume that the single scatter albedo, surface albedo and optical depth have been obtained by other means[35] and that the only part of the aerosol single scatter properties that we wish to retrieve is the phase matrix, **P**(θ), so **X=P**(θ). In this case if we use eq.(1), neglect the interaction between the molecular layer and the aerosol layer [third term on the right hand side of eq.(1)] and assume the downwelling radiation scattered by the aerosols is well approximated by single scattering, then the functional derivative in eq.(9) has the simple form

$$\left[\frac{\delta D(X;\theta)s}{\delta X}\Big|_{X=X^0}\right]^{-1} = \frac{P(\theta)s}{D_{AER}(X^0;\theta)\exp(-\tau_{MOL}/\mu_0)s} \tag{10}$$

where the denominator is not a matrix inverse, but simply indicates that each element in $\mathbf{P}(\theta)\mathbf{s}$ should be divided by the corresponding element in $\mathbf{D}_{\mathbf{AER}}\mathbf{s}$. This simple form is only appropriate if we assume single scattering and neglect the interaction between the molecular layer and the aerosol layer. Under any other assumption the functional derivative is non-local in angle and in coupling between elements of the Stokes vector, as one would expect for multiple scattering. It is important to recall when dealing with the analysis of polarization that the measurements and multiple scattering calculations are in the local meridional plane, while the phase matrix is specified in the scattering plane. In the implementation of this algorithm we rotated all quantities into the scattering plane. The fact that the approximation for the functional derivative given by eq.(10) applies to $\mathbf{P}(\theta)\mathbf{s}$ (in the scattering plane) means that only four elements of the phase matrix are estimated in this algorithm. In fact for assemblies of randomly oriented particles each having a plane of symmetry and for assemblies containing particles and their mirror particles in equal numbers two of these elements are identically zero[24, 33]. Thus we are actually only using the first two elements in the Stokes vector (**I,Q**) in this algorithm.On substituting eq.(10) into eq.(9) we obtain an expressionfor the iterative retrieval of the aerosol phase function from measurements of multiply scattered light given by,

$$P^n(\theta)=P^{n-1}(\theta)[1+\frac{d^m(\theta)-D(X^{n-1};\theta)S}{D_{AER}(X^{n-1};\theta)\exp(-\tau_{MOL}/\mu_0)S}] \quad (11)$$

A useful modification to this expression is[4] the introduction of the relaxation parameter C, viz.,

$$P^n(\theta)=P^{n-1}(\theta)[1+C\frac{d^m(\theta)-D(X^{n-1};\theta)S}{D_{AER}(X^{n-1};\theta)\exp(-\tau_{MOL}/\mu_0)S}] \quad (12)$$

The modification of the phase function calculated from eq.(11) is often too large and the iteration of the equation unstable. This is because the expression (10) for the functional derivative is only an approximation and when the misfit between the data and the model are large the first order Taylor expansion (8) is no longer valid, The parameter C in eq.(12) is usually set at some value less than unity, which can be based on the misfit between the data and the model so that unstable modifications to the phase function are avoided.

The result of each successive iteration of eq.(12) is an estimate of the phase matrix at a limited number and range of angles. In order to continue the iteration it is necessary to construct a phase matrix for the complete range of scattering angles. The method of interpolation and extrapolation[4] cannot be used here since even using the "three by three" approximation to calculate polarized light scattering[10,24] eq.(12) does not provide an estimate of all the required elements of the phase matrix. The method we use is that described in Section 2.2 above. The aerosol size and refractive index distribution is estimated from the limited range and number of measurements using eq.(5) and the complete phase matrix is then constructed from this size distribution[7]. The complete inversion algorithm therefore functions as follows.

1) Use a database, or other complementary measurements to find a plausible starting point for the inversion algorithm.

2) Use the difference between the observed and calculated radiance and polarization measurements to update those elements and scattering angles of the phase matrix that are observed, eq.(12).

3) Infer a size distribution and a refractive index from the updated phase matrix estimate, eq.(7).

4) Use the retrieved size distribution and refractive index to calculate the phase matrix., eq.(2).

5) Perform a multiple scattering calculation using the calculated phase matrix.

6) Return to step 2) until errors are sufficiently small (eg. χ^2 criteria), or convergence is too slow to justify further iterations.

3. SIMULATED RETRIEVALS

We have performed radiative transfer simulations of our multiple scattering inversion algorithm for a number of different phase functions and have attempted to obtain size resolved refractive index estimates and size distributions. We simulated the downwelling radiation at the bottom of the atmosphere using the atmospheric radiative transfer model described in Section 2.1 for almucantar scans at a solar zenith angle of 60° for azimuth angles between the sun and the direction of observation of from 5 to 180° in equally spaced 5° increments. To make sense of the large number of retrieved parameters we calculated the average refractive index for each of the nineteen log normal size distributions and then summed all the contributions from each of the log normal size distributions, for a particular size, with different refractive indices together.

In the first simulation we attempted to retrieve the Haze L size distribution with a refractive index of 1.33 for a wavelength of 0.7μm. The distribution of scattering properties was the test case used by de Haan *et al.*[24] which has a molecular scattering optical depth of 0.1 above a mixed aerosol (80%) and molecular (20%) layer of optical depth 0.5 above a Lambertian surface of albedo 0.1. This retrieval is particularly difficult since the refractive index is in fact not part of the available database of single scattering results (1.35 is the smallest), the Haze L distribution is very broad and the optical depth of molecular

scattering is relatively large and mixed with the aerosol. Figures 4a and 4b show the intensity and polarization of skylight for the Haze L test case (solid line) and the retrieved intensity and polarization (dashed line). Figures 4c and 4d show the Haze L phase function and degree of linear polarization (solid line) and the retrieved phase function and degree of linear polarization (dashed line). The intensity errors in Figure 4e are shown as a fractional error between the simulated and retrieved radiances (solid line) and phase function (dashed line). The polarization errors shown in Figure 4f are simply the differences in polarization between the simulated and retrieved polarization (solid line) and the degree of linear polarization (dashed line). The retrieved refractive index is 1.35 (only particles with a refractive index were retrieved), which is as good as can be expected and the effective radius that is retrieved is 0.441μm, while the actual effective radius of a Haze L distribution is 0.481μm. To demonstrate why the effective radius (which is the third moment of the size distribution divided by the second moment) is well retrieved we show in Figure 5a the size distribution multiplied by r^3 (solid line) and the retrieved size distribution multiplied by r^3 (dashed line). This figure also shows that the reason the phase function and polarization are not very well modelled is because the retrieved size distribution is far too narrow.

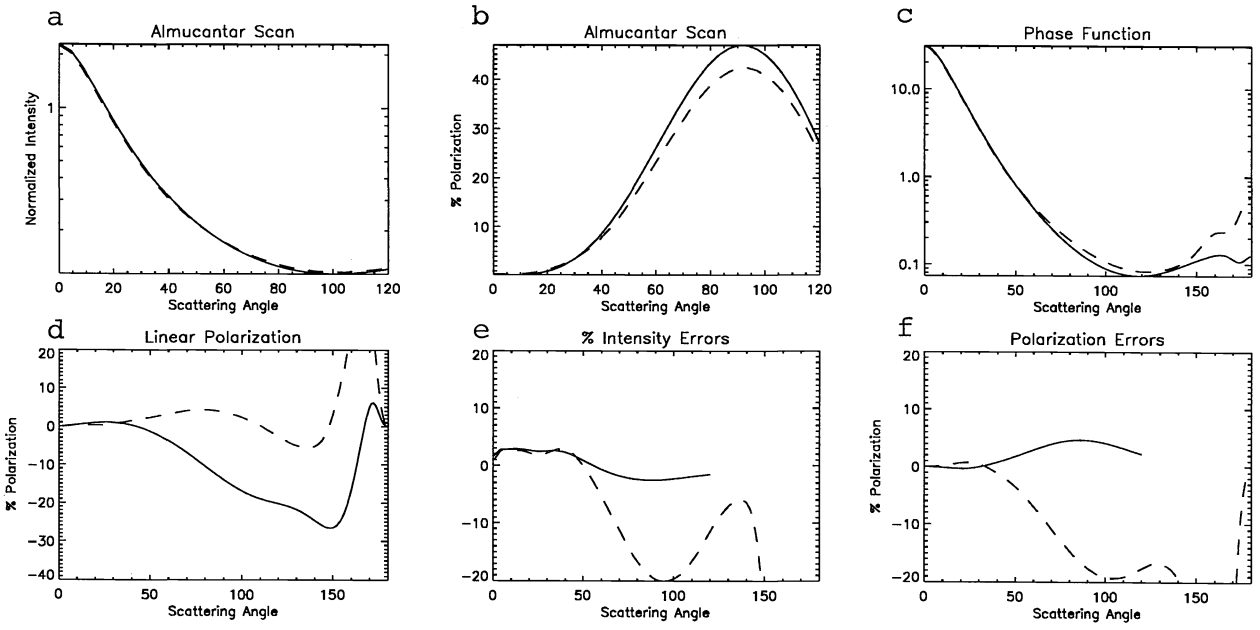

Figure 4. Haze L model phase matrix. a) Downwelling intensity for model (solid line), retrieved (dashed line). b) Polarization of downwelling radiation for model (solid line), retrieved (dashed line). c) Phase function of model (solid line), retrieved (dashed line). d) Phase matrix elements 100xP21/P11 of model (solid line), retrieved (dashed line). e) Fractional error x100 in retrieved downwelling intensity (solid line), fractional error x100 in retrieved phase function (dashed line). f) Error in retrieved polarization of downwelling radiation (solid line), error in retrieved phase matrix element 100xP21/P11 (dashed line).

The second simulation we performed is for a bimodal size distribution with the smaller mode having a mode radius of 0.2μm and a refractive index of 1.45 (simulating the accumulation mode of sulfate/nitrate) and the larger mode having a mode radius of 3.0μm and a refractive index of 1.4 (simulating the coarse mode of sea salt). The simulation was performed for a wavelength of 0.678μm, which is one of the wavelengths available using the PPR instrument, with a molecular layer of the appropriate Rayleigh scattering optical depth of 0.0416 above an aerosol layer of optical depth 0.5 above a Lambertian surface of albedo 0.1. Figure 6 shows the same set of figures as Figure 4, but for the bimodal size distribution. In Figures 6e and 6f we see that the downwelling intensity is retrieved to better than 1.0% and the polarization of the downwelling radiation is retrieved to better than 0.5%. The phase function is retrieved to an accuracy of better than 2% over most of the domain of observation and the single scattering degree of linear polarization is also retrieved to better than 2%. Figure 5b shows the size distribution (solid line) and that part of the size distribution that we would "expect" to retrieve (dashed line). The part that we would "expect" to retrieve (dashed line) has a small mode with a refractive index of 1.45(+/-0.02) and a larger mode

with a refractive index of 1.4(+/-0.02). Unfortunately a spurious distribution of particles with a refractive index of 1.55 is also retrieved (dot-dashed line in Fig. 5b).

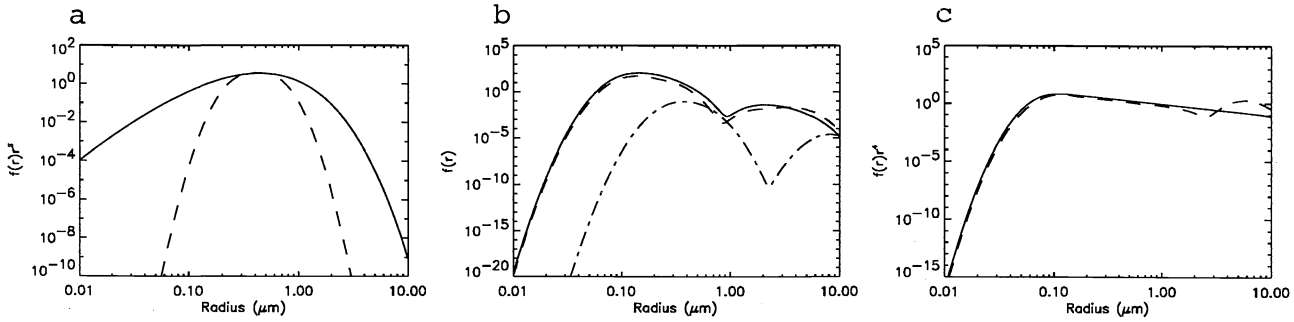

Figure 5. Size (weighted) distributions for a) Haze L distribution, b) Bimodal distribution, c) Power law distribution.

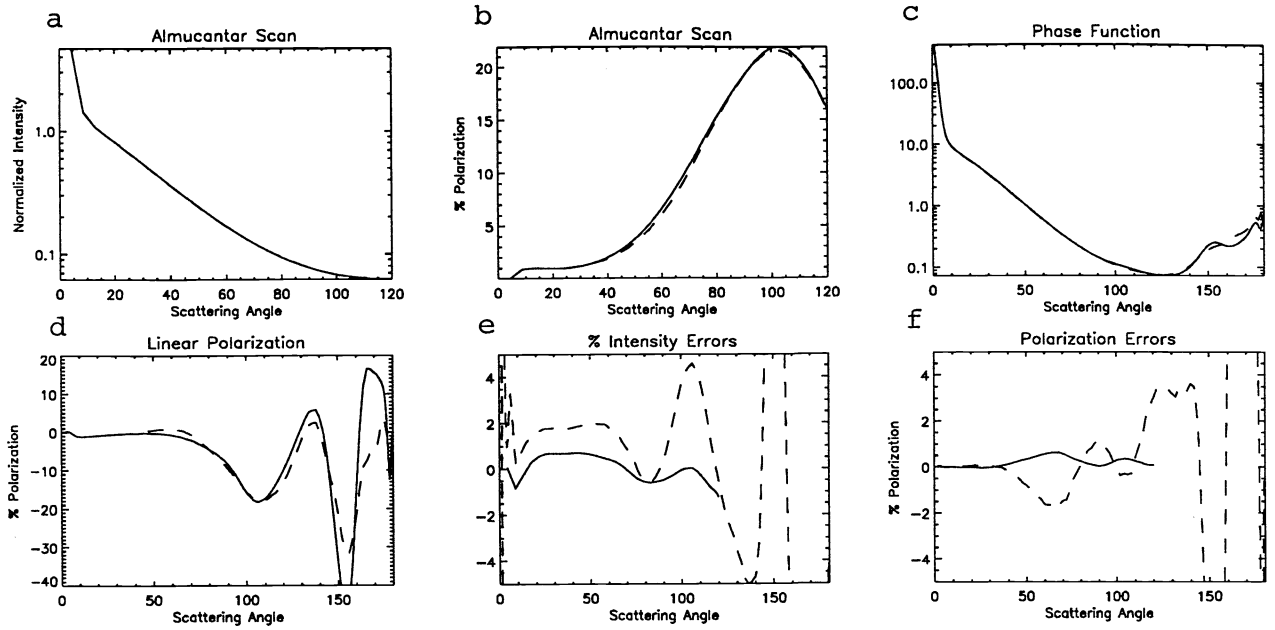

Figure 6. Similar to Figure 4, but for a bimodal size distribution.

The final simulation we performed was for a power law distribution with a refractive index of 1.45 at a wavelength of 0.678μm. The surface albedo, aerosol and molecular optical depths and their distribution were the same as for the bimodal size distribution simulation discussed above. The size distribution multiplied by r^4 is shown as a solid line in Figure 5c for comparison with other power law distributions and typical volume size distributions, $v(r)=4\pi r^4 f(r)/3$. The retrieval of downwelling intensity and polarization and the phase function and the degree of linear polarization are extremely good for this size distribution, see for example Figures 7e and 7f. The size distribution itself is also quite well retrieved as is seen from the dashed line in Figure 5c, which is the size distribution multiplied by r^4. The only error in the estimate of the size distribution is an overestimation of the number of large particles. However, although the refractive index is retrieved extremely accurately (+/-0.02) for sizes smaller than 0.5μu, for sizes larger than this there are erroneous refractive index retrievals. This is presumably because there are so few of these larger particles that very little of the downwelling light scatters off them.

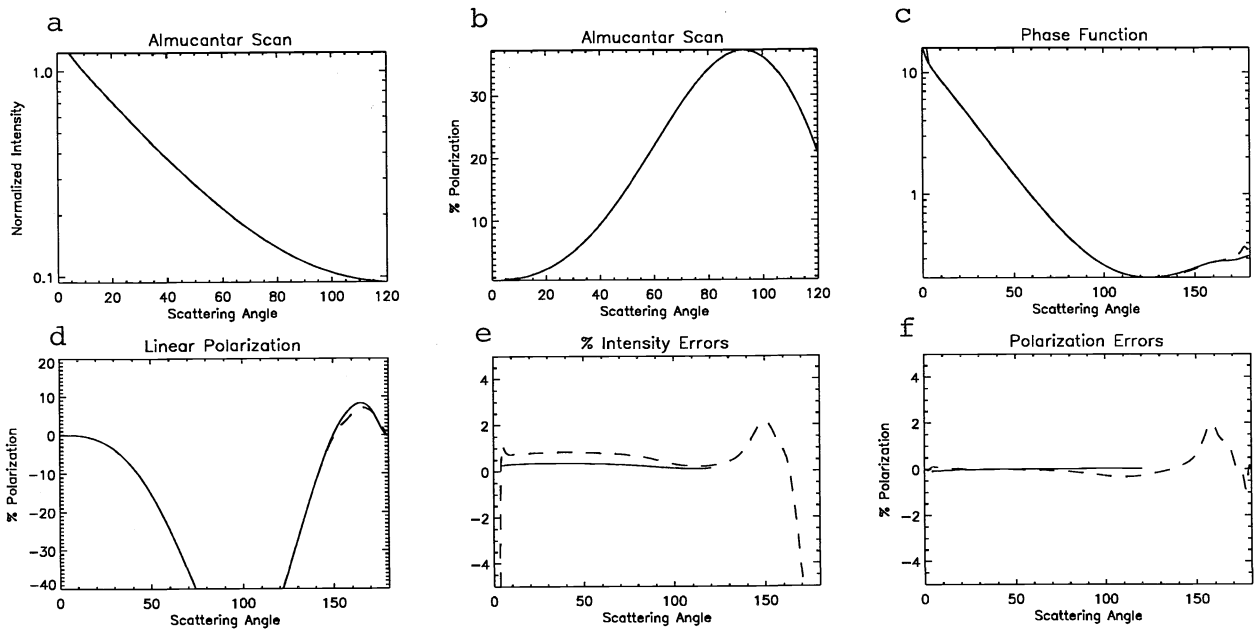

Figure 7. Similar to Figure 4, but for a bimodal size distribution.

4. CONCLUSIONS

The verisimilitude of the size distributions and refractive indices retrieved from the intensity and polarization of multiply scattered downwelling radiation using our algorithm is extremely good, see for example Figure 5. The poor retrieval for the Haze L distribution is presumably due to the large Rayleigh optical depth used in this test case and the fact that eq.(10) is not strictly applicable to a lower layer containing mixed aerosol and molecular scattering. Evidently the fact that this retrieval of the size distribution was so poor while the other retrievals were extremely good demonstrates that more extensive tests of the algorithm presented here are required to better understand the abilities and limits of the method. Even so, the fact that the correct effective radius and refractive index were found for the Haze L distribution is very encouraging. The accurate retrieval of a bimodal distribution for which the two modes have different refractive indices is impressive, though the spurious, high refractive index, particles that are also retrieved indicate that it is not necessarily possible to separate out different refractive index modes without error. The final retrieval of a power law size distribution indicates that for sizes for which the number density of particles is very small compared to the modal number density it may not be possible to retrieve the refractive index and that spuriously large numbers of large particles may be retrieved[7].

REFERENCES

1. Hansen, J.E., and A.A. Lacis, Sun and dust vs. greenhouse gases; an assessment of their relative roles in global climate change, *Nature*, **346**, 713-719, 1990.

2. J.E. Penner, R.J. Charlson, J.M. Hales, N.S. Laulainen, R. Leifer, T. Novakov, J. ogren, L.F. Radke, S.E. Schwartz, and L. Travis, Quantifying and minimizing uncertainty of climate forcing by anthropogenic aerosols, *BAMS*, **75**, 375-400, 1994.

3. J.E.Hansen, W. Rossow, and I. Fung, Long-Term Monitoring of Global Climate Forcings and Feedbacks, NASA Conf. Publ. 3234, NASA/GSFC 1993.

4. M. Wang and H.R. Gordon, Retrieval of the columnar aerosol phase function and single-scattering albedo from sky radiance over the ocean: simulations. *Appl. Opt.*, **32**, 4598-4609 1993.

5. M.I. Mishchenko, L.D. Travis, A.A. Lacis and B.E Carlson, Satellite remote sensing of nonspherical tropospheric particles. *Proc. SPIE*, 2311, 150-161, 1994.

6. M. Wendisch and W. von Hoyningen-Huene, High speed version of the method of 'successive order of scattering' and its application to remote sensing. *Beitr. Phys. Atmosph.*, 64, 89-91, 1991.
7. T. Nakajima, G. Tonna, R. Rao, P. Boi, Y.J. Kaufman, and B.N. Holben, Use of sky brightness measurements from ground for remote sensing of particulate polydispersions. *Appl. Opt.*, **35**, 2672- 2686, 1996.
8. B.N. Holben, T.F. Eck, I. Slutsker, D. Tanre., J.P. Buis, A. Setzer, E. Vermote, J.A. Reagan, Y.J Kaufman, T. Nakajima, F. Levenu, I. Jankowiak and A. Smirnov, Automatic sun and sky scanning radiometer system for network aerosol monitoring, *Remote Sens. Env.*, submitted, 1997.
9. B.N. Holben and D. Tanre, personal communication, 1997.
10. J.E. Hansen and L.D. Travis, Light scattering in planetary atmospheres, *Space Sci. Rev.*, **16**, 527-610, 1974.
11. T. Nakajima et al., Aerosol optical characteristics in the yellow sand events observed in May, 1982 at Nagasaki - Part II Models, *J. Meteorol. Soc. Japan*, **67**, 279-291, 1989.
12. M.I. Mishchenko, Light scattering by size-shape distributions of randomly oriented axially symmetric particles of a size comparable to a wavelength, *Appl. Opt.*, **32**, 4652-4666, 1993.
13. B.M. Herman, S.R. Browning and R.J. Curran, The effects of atmospheric aerosols on scattered sunlight, *J. Atmos. Sci.*, **28**, 419-428, 1971.
14. K.L. Coulson, *Polarization of intensity and light in the atmosphere,* Deepak Publishing, Hampton, VA., 1988.
15. A.I. Ivanov, G.Sh. Livshitz and E.L. Tem, Seasonal variation of albedo of a region by skylight polarization measurements in *Scattering and Absorption of Light in the Atmosphere*, Nauka, Kazakh SSR, 56-58 (in Russian) 1971.
16. G. Steinhorst, Stratospheric aerosol concentrations determined by an iterative method from twilight polarization measurements, *Contrib. to Atm. Phys.*, **50**, 508-523, 1977.
17. M.Z. Hansen, Atmospheric particulate analysis using angular light scattering. *Appl. Opt.*, **19**, 3441-3448, 1980.
18. V.V Veretennikov, V.S. Kozlov, I.E. Naats and V.Ya. Fadeyev, On the determination of the optical constants and microstructure of smoke aerosols from optical polarization measurements. *Izv. Atmos. Oceanic Phys.*, **16**, 177-181, 1980.
19. M. Tanaka, T. Nakajima and T. Takamura, Simultaneous determination of complex refractive index and size distribution of airborne and water-suspended particles from light scattering measurements, *J. Meteorol. Soc. Japan*, **60**, 1259-1272, 1982.
20. Y.J. Kaufman, R.S. Fraser and R.A. Ferrare, Satellite measurement of large-scale air pollution: Methods. *J. Geophys. Res.*, **97**, 9895-9909, 1990.
21. d'Almeida, G.A., P Koepke and E.P. Shettle, *Atmospheric Aerosols: Global Climatology and Radiative Characteristics*, Deepak Publishing, Hampton, VA., 1991.
22. G.W. Grams, I.H. Blifford Jr., D.A. Gillette, and P.B. Russell, Complex index of refraction of airborne soil particles. *J. Appl. Meteorol.*, **13**, 459-471, 1974.
23. Wiscombe, W.J., Improved Mie scattering algorithms, *Appl. Opt.*, **19**, 1505-1509, 1980.
24 J.F. de Haan, P.B. Bosma and J.W. Hovenier, The adding method for multiple scattering calculations of polarized light. *Astronom.Astrophys.*, 183, 371, 1987.
25. M.I. Mishchenko, A.A. Lacis, and L.D. Travis, Errors induced by the neglect of polarization in radiance calculations for Rayleigh-scattering atmospheres, *J. Quant. Spectrosc. Radiat. Transfer*, **51**, 759-778, 1994.
26. Lacis, A.A., J. Chowdhary, M.I. Mishchenko and B. Cairns, Modeling errors in diffuse-sky radiation: Vector vs. scalar treatment. *Geophys. Res. Letts.*, submitted, 1997.
27. Yamamoto, G. and M. Tanaka, Determination of aerosol size distribution from spectral attenuation measurements, *Appl. Opt.*, **8**, 447, 1969.
28. M.D. King, Sensitivity of constrained inversions to the selection of Lagrange multiplier. *J. Atmos. Sci.*, **39**, 1356-1369, 1982.
29. U. Amato, M.F. Carfora, V. Cuomo, and C. Serio, Objective algorithms for the aerosol problem. *Appl. Opt.*, **34**, 5442-5452, 1995.
30. K.S. Shifrin and Zolotov, I.G. Spectral attenuation and aerosol particle size distribution. *Appl. Opt.*, **35**, 2114-2124, 1996.
31. G. Ward, K.M. Cushing, R.D., McPeters and A.E.S. Green, Atmospheric aerosol index of refraction and size-altitude distribution from bistatic laser scattering and solar aureole measurements, *Appl. Opt.*, **12**, 2585-2592, 1973.
32. Twomey, S., *Introduction to the mathematic of inversion in remote sensing and indirect measurements*, Elsevier, New York, NY., 1977.
33. H.C. van de Hulst, *Light scattering by small particles*, Academic Press, New York, 1980.
34. J. Stoer, On the numerical solution of constrained least square problems. *SIAM J. Num. Anal.*, **8**, 382-421, 1971.
35. King, M.D., Herman, B.M. Determination of the ground albedo and the index of absorption of atmospheric particulates by remote sensing. Part I: Theory, *J. Atmos. Sci.*, **36**, 163-173, 1979.